P-V-T equation of state of periclase from synchrotron radiation measurements

Agnès. Dewaele, Guillaume Fiquet, Denis Andrault, Daniel Hausermann

JOURNAL OF GEOPHYSICAL RESEARCH, VOL. 105, NO. B2, PAGES 2869–2877, FEBRUARY 10, 2000

P-V-T equation of state of periclase from synchrotron radiation measurements

Agnès Dewaele and Guillaume Fiquet

Laboratoire des Sciences de la Terre, École Normale Supérieure de Lyon, Lyon, France

Denis Andrault

Laboratoire des Géomatériaux, Institut de Physique du Globe de Paris, Paris, France

Daniel Hausermann

European Synchrotron Radiation Facility, Grenoble, France

Abstract. The volume of periclase (MgO) has been measured by monochromatic X-ray diffraction in a laser-heated diamond anvil cell up to a pressure of 53 GPa and a temperature of 2500 K. The X-ray source was synchrotron radiation at the European Synchrotron Radiation Facility (Grenoble, France). In addition to laser heating, the use of argon as a pressure transmitting medium provided quasi-hydrostatic conditions in the cell assembly. In order to take thermal pressure effect into account, pressure was measured using an internal pressure calibrant (platinum). By analysis of the experimental P-V-T data set the following parameters were obtained: at ambient temperature, $K_0' = 3.94 \pm 0.2$ when K_0 is fixed to 161 GPa (with a Birch-Murnaghan equation of state); under high temperature, $\alpha(P = 0, T) = (3.0 + 0.0012T) \times 10^{-5}$ K^{-1}; $(\partial K_T/\partial T)_P$ = -0.022(3) GPa K^{-1}. The quasi-harmonic Debye model appears to describe correctly the temperature dependence of the volume at high pressure within experimental errors, with the following parameters: $\theta_{D0} = 800$ K, $\gamma_0 = 1.45$ (Grüneisen parameter under ambient conditions), and $q = 0.8 \pm 0.5$.

1. Introduction

Periclase is a material of primary interest in geophysics, for two reasons: first, (Mg, Fe)O is proposed to be the second most abundant material in the Earth's lower mantle, so that the knowledge of its physical properties will help to understand deep Earth's physics; second, because of its large stability pressure (P) and temperature (T) domain, and its low chemical reactivity, MgO can be used as a pressure calibrant in high P and high T experiments.

Several experimental studies, based on various techniques, have been carried out to determine the thermoelastic parameters (K_T, K_S, α and their P and T derivatives) and the corresponding equation of state (EoS) of MgO. Its adiabatic elastic moduli (K_S and μ) and their pressure and temperature derivatives have been measured with acoustic waves velocity methods, up to 8 GPa and 1800 K [*Jackson and Niesler*, 1982; *Isaak et al.*, 1989; *Chen et al.*, 1998]. The EoS of MgO along the Hugoniot has been calculated from shock compression data [*Jamieson et al.*, 1982; *Duffy and Ahrens*, 1995]. EoS measurements have also been achieved under static conditions by X-ray diffraction in several types of high-pressure apparatus. For periclase, this was done for the first time in a diamond anvil cell in 1979, up to 95 GPa at room temperature [*Mao and Bell*, 1979]. Numerous other studies have followed in diamond anvil cells at ambient T [*Duffy et al.*, 1995; *Fiquet et al.*, 1996], externally heated diamond anvil cells (carried out on $(Mg_{0.6},Fe_{0.4})O$ [*Fei et al.*, 1992], up to 30 GPa and 800 K, or MgO [*Fei*, 1999], up to 65 GPa at 300 K and 25 GPa at 1100 K), or large volume apparatus up to 10 GPa and 1700 K [*Utsumi et al.*, 1998]. Available experimental bulk moduli data for MgO are summarized in Table 1. The vibrational spectroscopy measurements are difficult to perform on periclase because only one infrared mode can be observed; *Chopelas* [1990] measured vibronic bands in the fluorescence spectrum of Cr^{3+}-doped MgO to infer vibrational properties of that lattice.

As MgO is a simple example of close-packed oxide, it has also been widely theoretically studied. For instance, elastic properties of MgO have been evaluated at high pressure and 0 K by ab initio methods [*Mehl et al.*, 1988; *Karki et al.*, 1997], and its high-pressure thermal

Paper number 1999JB900364.
0148-0227/00/1999JB900364$09.00

Table 1. Summary of MgO Incompressibility (K_T) Measurements

Reference	Technique	P Range, GPa	T Range, K	K_T, GPa	K'_T
Jackson and Niesler [1982]	single crystal + sound velocity	0-3	300	160.3(3)	4.15(10)
Isaak et al. [1989]	single crystal + sound velocity	10^{-4}	300-1800	161.6	
Mao and Bell [1979]	DAC + X-ray diffraction	0-120	300	160	4.7
Duffy et al. [1995]	DAC + X-ray diffraction	0-227	300	177(4)	4.0(1)
Fiquet et al. [1996]	DAC + X-ray diffraction	0-18	300	162(2)	4.0
Utsumi et al. [1998]	multianvils + X-ray diffraction	0-10	300-1700	153(3)	4.0
Fei [1999]	DAC + X-ray diffraction	0-65	300-1100	160(2)	4.0

The values of K_T and K'_T are taken at 0 GPa and 300 K. In all static compression studies, the Birch-Murnaghan EoS is used, except for the *Mao and Bell* [1979] study. Error bars are reported when available. DAC, Diamond Anvil Cell.

properties have also been ab initio calculated within a quasi-harmonic approximation [*Isaak et al.*, 1995], or in an anharmonic framework [*Inbar and Cohen*, 1995]. The validity of these calculations needs to be tested against experimental measurements over a large P-T range.

We report here MgO volume measurements performed in a CO_2 laser heated diamond anvil cell up to 53 GPa and 2500 K on the high-pressure beamline (ID30) at the European Synchrotron Radiation Facility, Grenoble, France. These measurements extend the scanned P-T range for an accurate determination of high P and high T EoS of MgO. The experimental P-V-T data set is used to constrain the parameters of high temperature EoS.

2. Experiment

2.1. Experimental Apparatus

The experimental high-pressure and high-temperature setup has been described previously by *Fiquet et al.* [1998]. In these experiments the monochromatic X-ray synchrotron beam and an infrared laser beam were both focused on the sample in a Chervin-type diamond anvil cell [*Chervin et al.*, 1995].

Laser heating has been achieved by a high power CO_2 laser, focused on the sample and forming a 60 μm diameter hot spot. Thermal emission spectra of the sample during heating were collected by a set of two lenses and dispersed by a 150 g.m^{-1} grating spectrometer coupled with a Charge Coupled Device detector.

The X-ray beam was focused by two mirrors and filtered by a 20 μm diameter pinhole to form a 10 x 15 μm size spot on the sample. Diffracted signal was collected on an imaging plate and scanned using a special device, the FastScan detector [*Thoms et al.*, 1998]. This detector allows on-line reading and transfer of one two-dimensional (2-D) X-ray pattern in a typical time of 12 s. This device is very useful for such P-V-T measurements because several images can be recorded without change in sample position or in optical alignment. Beam wavelength ($\lambda = 0.42416$ Å) and sample to imaging plate distance (309.2 mm) have been adjusted using Sn absorption edge and the diffracted pattern of Si.

2.2. Sample Loading

High-purity synthetic MgO was mixed with platinum black (PROLABO product) used as a pressure calibrant. As the atomic X-ray scattering factor is proportional to the atomic number, a very small amount of platinum (volumic ratio of the order of 1 to 20) could provide a high-intensity diffracted signal. Samples were loaded in a gasket with liquid argon, while the cell was placed inside a cryostat immersed in liquid nitrogen. Indented rhenium gaskets (thickness 50 to 60 μm) with 100 μm diameter holes were used. The sample to argon volume ratio was approximately 1 to 5 when the gasket sealed against the diamonds. Argon was used to provide quasi-hydrostatic stress conditions in the pressure chamber.

Two-dimensional diffracted patterns consisting of spotty powder rings were angularly integrated with the fit2D program [*Hammersley*, 1996] to obtain a 1-D spectrum. We used the GSAS program package [*Larson and Van Dreele*, 1994] to refine the lattice parameters of each phase [see *LeBail*, 1992].

For typical diffraction spectra, five phases were needed to explain all diffraction lines: MgO and Pt (the most intense), and face centered cubic (fcc) argon, hexagonal closed packed (hcp) argon, and δ-N_2 (Figure 1). The δ-N_2 peaks show that liquid nitrogen entered the cell during the loading process, probably because of a leak in the cryostat. The fcc-argon and δ-N_2 are the thermodynamically stable phases of argon and nitrogen in the scanned P-T domain [see *Ross et al.*, 1986; *Mills et al.* 1986]. However, in the Ar-N_2 binary system, the hcp modification has been observed at ambient pressure, when argon is mixed with small amounts of N_2 [*Barrett and Meyer*, 1965]. As we also observed in our experiments, the latter authors note that molar volume of the (Ar + N_2) hcp phase is slightly higher than the molar volume of a pure fcc-argon phase in the same $P-T$ conditions. The Ar-N_2 system seems therefore to have the same qualitative behavior under ambient and

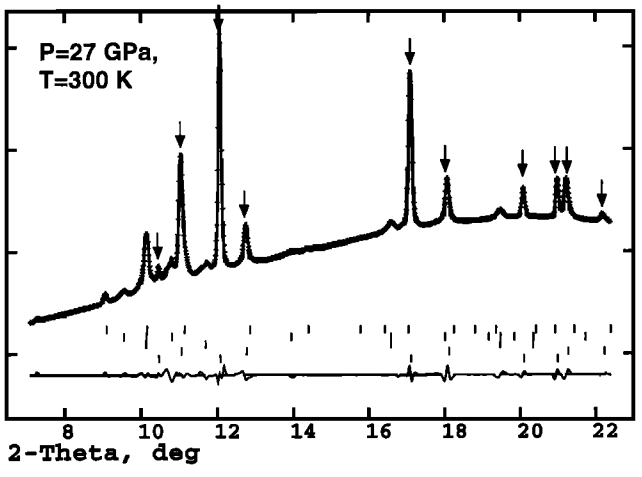

Figure 1. Typical angle dispersive X-ray diffraction pattern of the sample assembly (MgO + Pt + pressure transmitting medium) obtained at 27 GPa and 300 K. Shaded pluses represent the observed profile, and the solid black line represents a synthetic profile obtained from a LeBail refinement. Reflexion angles for the present phases are represented by ticks: MgO (Fm3m group), Pt (Fm3m), fcc-Ar (Fm3m), hcp-Ar (P63/mmc), and δ-N_2, from bottom to top. On the bottom line is the difference between the experimental and the synthetic profile.

high pressure. *Wittlinger et al.* [1997] have reported evidence for hcp-Ar under high pressure in a cryogenically loaded diamond anvil cell, but only in some of their loadings. We suggest that their observation of the hcp modification was also caused by a nitrogen leak. In the diamond anvil cell, the surfaces between diamond or gasket and pressure transmitting medium could allow an epitaxial growth of the observed hcp argon.

2.3. Temperature and Pressure Measurements

Temperature was evaluated by the analysis of thermal emission spectra of the sample, recorded during the exposure of the imaging plate. The procedure was as follows: the thermal emission spectrum of forsterite at 2163 K recorded in the same optical configuration is used to extract the frequency response $H(\lambda)$ of the optical assembly, assuming that forsterite behaves as a perfect gray body. Thermal emission spectra were divided by $H(\lambda)$ and fitted against a perfect gray body spectrum by least squares techniques, with temperature and emissivity of the sample as free parameters. Several spectra recorded during the exposure of an imaging plate (in 0.5 to 3 min) exhibit small T variations: less than $\pm$50 K. However, the assumption that the frequency dependence of the sample emissivity is the same for forsterite and for the sample could bias the measurements, introducing an uncertainty of the order of 100 to 150 K. We expect therefore an uncertainty of the order of $\pm$200 K in the temperature measurement.

It has been recently shown that pressure locally increases in the laser-heated spot in diamond anvil cells [*Fiquet et al.*, 1996; *Andrault et al.*, 1998; *Dewaele et al.*, 1998]. It follows that pressure can not be precisely estimated by the ruby fluorescence measurement method, as the ruby chip must be located outside of the laser-heated spot. We have therefore used in situ high-temperature pressure calibrant: a material of known EoS is mixed with the sample, and its volume is measured under the same P-T conditions. Pressure is then deduced from the pressure calibrant volume. This approach relies on the assumption that stresses are uniform at the grain size scale. The P-V-T EoS of platinum has been determined by the use of measured shock wave Hugoniot data for this material, coupled with a Debye model (see *Jamieson et al.* [1982] for the method and the parameters of the calculation). Although the gold EoS has been more accurately determined [*Jamieson et al.*, 1982], we chose platinum because of its high melting point (700 K higher than gold at ambient pressure).

Sixty one P-V-T points were measured (Table 2). According to *Jamieson et al.* [1982], the typical relative uncertainty on the volume determined via shock wave velocities is about 0.1%. The corresponding pressure uncertainty is around 3%. Since the Hugoniot temperatures remain relatively low for platinum (300 to 600 K at 0 to 50 GPa), this pressure uncertainty is characteristic of the ambient temperature measurements. Pressure uncertainty is greater at high T because of possible errors on the thermal pressure calculation for the platinum EoS. With α and K_T values for platinum at ambient conditions and assuming a 5% error in thermal pressure, we obtained the following uncertainty in pressure: $\Delta P = 3 \times 10^{-2} P + 4 \times 10^{-4}(T - T_0)$ (P in GPa, T in K). This error was used in the following analysis of the experimental measurements.

Following *Singh* [1993], we have estimated the deviatoric stresses in the sample using the ratio between a_{220} and a_{200} for MgO, in several ambient temperature or high-temperature spectra. Elastic parameters measured under high pressure and ambient temperature by Brillouin scattering method (*J. D. Bass*, personal communication, 1998) have been used. If σ_3 and σ_1 are positive vertical and radial strains, respectively, in the diamond anvil cell, we obtained that under the Reuss assumption, $\tau = (\sigma_3 - \sigma_1)/2 \simeq 1 \pm 1$ GPa in these experiments.

3. Ambient Temperature Measurements

MgO volume as a function of pressure at ambient temperature (T_0) is plotted in Figure 2. The volumes measured by *Mao and Bell* [1979] are higher than our current measurements at pressure greater than 40 GPa. As discussed by several authors [e.g., *Jackson and Niesler*, 1982; *Duffy et al.*, 1995], this discrepancy can be explained by the possible existence of non hydrostatic stresses in the *Mao and Bell* [1979] study. We therefore do not use their measurements for the following analysis of the ambient T EoS.

Table 2. Experimental P-V-T Data Points for MgO

T, K	Pt:a, Å	P, GPa	MgO:V, Å^3
2015	3.8824	20.5(1.2)	70.816(7)
2227	3.8912	19.7(1.3)	71.287(10)
2474	3.8949	21.3(1.5)	71.765(7)
2188	3.8787	22.5(1.4)	70.607(4)
2000	3.8685	23.9(1.4)	70.061(8)
2349	3.8748	24.5(1.6)	70.709(8)
1900	3.8394	31.3(1.6)	67.626(5)
2008	3.8404	31.7(1.6)	67.913(6)
2097	3.8434	31.4(1.7)	67.412(4)
1964	3.7758	53.0(2.2)	62.390(4)
1750	3.8563	25.5(1.3)	68.441(2)
2000	3.8642	25.0(1.4)	68.921(4)
1934	3.8667	24.0(1.4)	69.183(3)
2110	3.8720	23.7(1.4)	69.593(4)
2160	3.8720	24.0(1.4)	69.592(4)
1750	3.8959	15.5(1.0)	71.649(6)
1927	3.8980	16.2(1.1)	71.923(5)
1865	3.9077	13.6(1.0)	72.433(4)
1870	3.7770	51.86(2.2)	62.362(3)
1928	3.7761	52.6(2.2)	62.050(6)
1900	3.7770	52.1(2.2)	62.368(6)
2223	3.8042	44.5(2.1)	64.301(4)
2050	3.8066	42.6(2.0)	64.369(4)
2064	3.8079	42.2(2.0)	64.481(6)
1950	3.8077	41.5(1.9)	64.394(7)
1908	3.7783	48.0(2.1)	63.146(4)
2066	3.7905	48.4(2.2)	62.866(6)
2067	3.7903	48.2(2.2)	63.004(10)
2050	3.7902	48.2(2.2)	63.151(6)
1966	3.7770	52.5(2.3)	62.306(3)
1849	3.7773	51.6(2.3)	62.204(3)
1980	3.8480	29.3(1.6)	67.894(4)
1950	3.8507	28.3(1.5)	68.242(6)
2040	3.8136	35.0(1.8)	66.246(10)
1975	3.8138	35.0(1.8)	66.025(8)
2250	3.8279	37.0(1.8)	66.303(7)
2210	3.8344	34.8(1.7)	66.468(5)
2320	3.8372	34.7(1.8)	66.606(7)
2374	3.8401	34.2(1.8)	66.782(11)
2315	3.8484	31.4(1.8)	67.515(12)
2200	3.8064	43.6(2.1)	64.274(5)
300	3.7919	36.2(1.1)	63.687(4)
300	3.7835	39.2(1.2)	62.663(3)
300	3.7689	44.7(1.4)	61.778(3)
300	3.8276	24.3(0.7)	66.118(4)
300	3.8438	19.5(0.6)	67.608(2)
300	3.8572	15.7(0.5)	68.798(2)
300	3.8679	12.9(0.4)	69.696(4)
300	3.9191	00.8	74.130(4)
300	3.8734	11.5(0.4)	70.139(2)
300		00.0	74.744(10)
300	3.8594	15.1(0.5)	69.182(8)
300	3.8492	17.9(0.5)	68.392(3)
300	3.8334	22.6(0.7)	66.874(6)
300	3.8126	29.1(0.9)	65.168(3)
300	3.7994	33.5(1.0)	63.786(3)
300	3.7971	34.3(1.1)	63.891(8)
300	3.8386	20.0(0.6)	67.226(3)
300	3.8388	21.0(0.7)	67.332(5)
300	3.8203	26.6(0.8)	65.637(2)
300	3.8187	27.1(0.8)	65.544(6)

Temperature uncertainties are ± 200 K. Uncertainties on volume are calculated by the GSAS program.

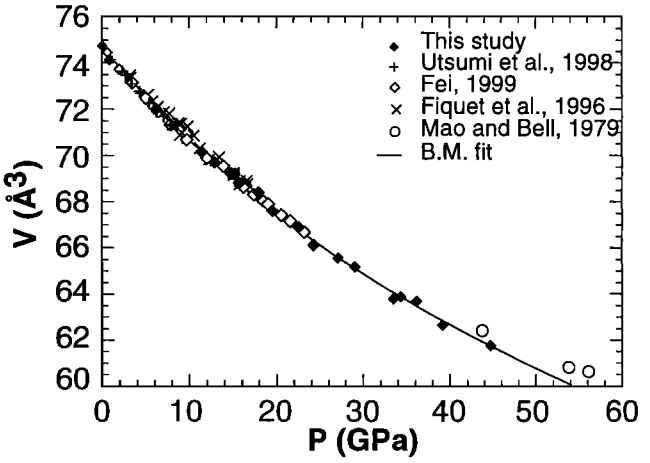

Figure 2. Ambient temperature compression curve of MgO, plotted with previous measurements. The solid line represents the Birch-Murnaghan fit of all measurements, except *Mao and Bell* [1979] data, leading to $K_0' = 3.94$, with $K_0 = 161$ GPa and $V_0 = 74.71$ Å^3.

The ambient temperature P-V measurements are described by a third-order Birch-Murnaghan equation of state. This equation relies on a third-order development of the free energy of a compressed material with an Eulerian description of stresses and strains. The pressure at a given T (here T_0) is given by

$$P(V,T_0) = \frac{3}{2}K_0\left(\left(\frac{V_0}{V}\right)^{\frac{7}{3}} - \left(\frac{V_0}{V}\right)^{\frac{5}{3}}\right) \times \left(1 + \frac{3}{4}(K_0' - 4)\left(\left(\frac{V_0}{V}\right)^{\frac{2}{3}} - 1\right)\right), \quad (1)$$

where K_0, K_0', and V_0 are incompressibility, its pressure derivative, and volume, at ambient pressure, respectively. This EoS is widely used in geophysics because it describes the compression of many materials with only three measured parameters: V_0, K_0 and K_0'. Several others EoS have been proposed, however, and are often expressed using the same parameters in different ways (see below). None of these EoS has been well established, and the physical meaning of V_0, K_0, and K_0' could be doubtful. If that was the case, they should be considered as nonindependent fitted parameters (see the well-known K_0/K_0' trade-off by *Mao et al.* [1991], for example), and extrapolation in T and P of measured EoS to higher pressure would be impossible.

However, the fitted K_0 value can be confronted with both ultrasonic or Brillouin scattering measurements, to test its physical meaning. It has been shown that for several materials, K_0 and V_0 values provided by static compression measurements can be reconciled with acoustic data (see Table 1 for MgO, *Jeanloz and Hemley* [1994] for $MgSiO_3$-perovskite, and *Knittle* [1995] and *Anderson et al.* [1992] for CaO, for instance).

The case of K_0' is more ambiguous, because this parameter is the most affected by the truncation in (1).

Indeed, some discrepancies between acoustic and compression measurements values of this parameter have been reported (e.g., for CaO by *Richet et al.* [1988]). For this reason, while analyzing the compression data, we chose to fix the K_0 value, which seems to be correctly constrained for MgO by acoustic measurements ($K_0 = 161 \pm 1$ GPa; see Table 1). In the same way, V_0 is also fixed to the average value of several measurements [*Dubrovinsky and Saxena*, 1997; *Mao and Bell*, 1979; *Duffy et al.*, 1995; *Fiquet et al.*, 1996]: $V_0 = 74.71 \pm 0.03$ Å^3. This value is also in good agreement with an ambient pressure extrapolation of the high pressure data points. The K'_0 value is obtained by a fit of all available measurements, except *Mao and Bell* [1979] values: the current data, as well as those of *Fiquet et al.*, [1996], *Fei* [1999], and *Utsumi et al.* [1998]. By this method, we obtain $K'_0 = 3.94 \pm 0.06$. Unfortunately, the present measurements are not sufficient to determine the pressure effect on K'_0. If the present data set alone is considered, $K'_0 = 3.91$ is obtained. Pressure uncertainties lead to $K'_0 = 3.94 \pm 0.2$. If K'_0 is fixed to 4.0, $K_0 = 159$ GPa is obtained (Table 3).

By comparison, other EoS functions have been used to determine K'_0 values, with the same fixed value of K_0 and V_0 (Murnaghan (M) EoS [see *Poirier*, 1991], logarithmic (L) EoS [*Poirier and Tarantola*, 1998], Vinet EoS (V) [*Vinet et al.*, 1987]). Results are presented in Table 3. In the measured pressure range (0-50 GPa), fitted K'_0 does not depend strongly on the choice of the EoS, except for M EoS (variations of less than 0.1 between the Birch-Murnaghan (BM), L and V EoS).

However, when these three EoS with the parameters listed in Table 3 are extrapolated to higher compression, pressures differ: for example, at $V/V_0 = 0.667$, pressures given by BM, V and L EoS are 145, 142, and 138 GPa, respectively. At this volume, incompressibilities K_T (642, 610, and 578 GPa, respectively) differ by more than 10%. If no higher pressure compression data exist, this large uncertainty must be considered in geophysical studies, that constrain the chemical and mineralogical composition of the deep Earth from comparison between experimental incompressibility and K_S profile deduced from seismological measurements [see, e.g., *Ita and Stixrude*, 1992]. Higher compression data are thus required to cover the whole P-T range of the lower mantle (23-135 GPa; 2000-3000 K).

Table 3. Set of Parameters for Different EoS Used to Fit Experimental Ambient T Compression Data for MgO

EoS	V_0, Å^3	K_0, GPa	K'_0
Birch-Murnaghan	74.71 (fixed)	159.0(6)	4 (fixed)
Birch-Murnaghan	74.71 (fixed)	161 (fixed)	3.94(5)
Murnaghan	74.71 (fixed)	161 (fixed)	3.75(5)
Vinet	74.71 (fixed)	161 (fixed)	4.01(5)
logarithmic	74.71 (fixed)	161 (fixed)	4.08(6)

The data are from *Utsumi et al.* [1998], *Fiquet et al.* [1996], *Fei* [1999], and from this study.

4. High Temperature Measurements

4.1. Birch-Murnaghan Formalism

At high temperature the same Birch-Murnaghan isothermal formalism can be used:

$$P(V,T) = \frac{3}{2} K_{0,T} \left(\left(\frac{V_{0,T}}{V} \right)^{\frac{7}{3}} - \left(\frac{V_{0,T}}{V} \right)^{\frac{5}{3}} \right) \times \left(1 + \frac{3}{4}(K'_{0,T} - 4) \left(\left(\frac{V_{0,T}}{V} \right)^{\frac{2}{3}} - 1 \right) \right), \quad (2)$$

where

$$V_{0,T} = V(P = 1 \text{ bar}, T)$$
$$V_{0,T} = V_0 \exp\left(\int_{T_0}^{T} \alpha(P = 1 \text{ bar}, T) dT \right),$$

and $K_{0,T}$ is assumed to behave as follows:

$$K_{0,T} = K_T(P = 1 \text{ bar}, T)$$
$$K_{0,T} \simeq K_0 + \left(\frac{dK_{0,T}}{dT} \right) (T - T_0).$$

We also assume that $K'_{0,T} \simeq K'_{0,T}(T_0) = K'_0$, because it is difficult to constrain the temperature dependence of $K_{0,T}$ and $K'_{0,T}$ at the same time. This is however a very restrictive assumption which will be discussed further.

4.1.1. Inversion of the P-V-T data. This EoS can be used in a generalized inversion of the P-V-T data [*Matas*, 1999]. The algorithm is based on a generalized gradient method. A linear behavior of the thermal expansion coefficient ($\alpha(P = 1 \text{ bar}, T) = \alpha_0 + \alpha_1 T$) is assumed. Three high P-T data sets have been used: *Utsumi et al.* [1998] data, *Fei* [1999] data, and the current measurements. K_0, K'_0, and V_0 have been fixed to 161 GPa, 3.94, and 74.71 Å, respectively. The $dK_{0,T}/dT$, α_0, and α_1 are treated as free parameters. In this algorithm, uncertainties in P and V can influence both error bars and values of the refined parameters. Errors previously discussed and given by Utsumi et al. and Fei are used. Fixed and refined parameters are listed in Table 4.

Thermal expansion factors, α_0 and α_1, are strongly correlated, and it is not possible to constrain both of them. For this reason we have fixed $\alpha_1 = 1.2 \times 10^{-8}$ K^{-2} (this value is in good agreement with the ambient P measurements of *Dubrovinsky and Saxena* [1997] and *Fiquet et al.* [1999]) in a second set of simulations.

Inversions carried out on our measurements alone and *Fei* [1999] (with gold as pressure calibrant) measurements yield the same $dK_{0,T}/dT$ value; -0.022 GPa K^{-1}, but that value is not compatible with the *Utsumi et al.* [1998] estimate (-0.032 GPa K^{-1}). We can explain this discrepancy as follows: (1) the T_0 elastic parameters

Table 4. Parameters Obtained by Inversion of Different Data Sets

Data set	T_0 Parameter	$\partial K_T/\partial T$, GPa K^{-1}	α_0, K^{-1}	α_1, K^{-2}
This study	161 GPa, 3.94	-0.020(3)	$2.6(5)\times10^{-5}$	$1.2(5)\times10^{-8}$
Utsumi et al. [1998]	153 GPa, 4.00[a]	-0.034(2)	$4.18(6)\times10^{-5}$	$0.2(1)\times10^{-8}$
Fei [1999]	161 GPa, 3.94	-0.022(1)	$3.2(5)\times10^{-5}$	$0.7(8)\times10^{-8}$
All data	161 GPa, 3.94	-0.021(1)	$3.49(5)\times10^{-5}$	$0.17(8)\times10^{-8}$
This study	161 GPa, 3.94	-0.022(1)	$2.9(3)\times10^{-5}$	1.2×10^{-8}[b]
Utsumi et al. [1998]	161 GPa, 3.94	-0.045(2)	$3.53(4)\times10^{-5}$	1.2×10^{-8}[b]
Fei [1999]	161 GPa, 3.94	-0.022(1)	$2.83(4)\times10^{-5}$	1.2×10^{-8}[b]
All data	161 GPa, 3.94	-0.026(1)	$2.9(2)\times10^{-5}$	1.2×10^{-8}[b]

In all inversions the T_0 EoS parameters (K_0, in GPa, and K_0') have been fixed. The thermal expansion coefficient under ambient pressure is expressed as $\alpha = \alpha_0 + \alpha_1 T$.

[a]Ambient temperature EoS reported in *Utsumi et al.* [1998].

[a]Fixed values.

from the study of Utsumi et al. differed from ours (K_0 = 153 GPa, $K_0' = 4$). This could suggest that the pressure calibration used by Utsumi et al., which is based on NaCl EoS, is not compatible with ours; (2) the value of $(\partial K_{0,T}/\partial T)_P$ could be sensitive to the pressure range studied, which is narrower in *Utsumi et al.*'s study (0 to 10 GPa) than in the present measurements, especially if $K'_{0,T}$ is temperature dependent.

It is also difficult to reconcile the current $dK_{0,T}/dT$ value (-0.022 GPa K^{-1}) with the *Isaak et al.* [1989] value (-0.030 GPa K^{-1}, averaged value between 300 and 1800 K measured by a resonance method). However, it is difficult to compare two parameters which have been determined in very different experimental conditions and physical contexts. The numerous assumptions currently and usually done concerning high P/high T EoS could explain the discrepancy between compression and acoustic data, which measure the true physical parameters.

Isaak et al. [1990] calculated that $\mathrm{d}K_{0,T}/\mathrm{d}T = -0.019$ GPa K^{-1} between 300 and 2000 K, using a fourth-order Birch-Murnaghan EoS, which is in correct agreement with our estimate.

4.1.2. Pressure dependence of the thermal expansion coefficient. We can easily calculate the value of the averaged thermal expansion coefficient (α_{av}) and study its variations with pressure. Variable α_{av} is calculated from

$$\alpha_{av}(P,T) = \frac{1}{T-T_0}\int_{T_0}^{T}\alpha(P,T)dT$$

$$\alpha_{av}(P,T) \simeq \frac{V(P,T)-V_{BM}(P,T_0)}{V_0(P,T_0)\,(T-T_0)},$$

where $V_{BM}(P,T_0)$ is obtained from the ambient temperature Birch-Murnaghan EoS, with previously discussed parameters (Figure 3). The expected uncertainty on α_{av} is around 15%. Some points measured by *Utsumi et al.*, 1998, largely deviate from the trend. Even if these points correspond to the lowest temperatures measurements, this deviation can not be explained by the thermal expansion coefficient temperature dependence alone (which disappears at high pressure [see, e.g., *Inbar and Cohen*, 1995]). We suggest that these few points could cause the high value of $|(\partial K_T/\partial T)_P|$ deduced from the Utsumi et al. data set.

For $P > 10$ GPa, α_{av} calculated from *Fei* [1999] measurements (at 1100 K, gold as pressure calibrant) is in good agreement with the current data (at 1800 K $< T <$ 2500 K). This confirms that α is only slightly temperature dependent under high pressure. The variations of current $\alpha_{av}(P,T)$ can be fitted by the following law:

$$\alpha_{av}(P,T) \simeq (3.2\times10^{-5} + 0.6\times10^{-8}T) \times(1 - 0.024P + 2.2\times10^{-4}P^2),$$

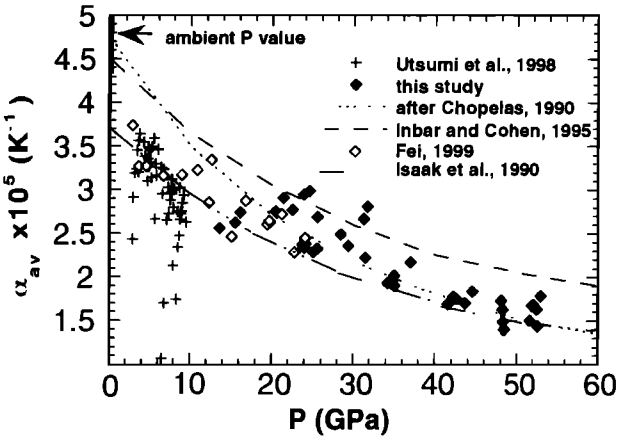

Figure 3. Averaged value (see text) of the thermal expansion coefficient of MgO as a function of pressure, from our P-V-T measurements and from *Utsumi et al.* [1998] measurements. The ambient P value is calculated in the same temperature range with *Dubrovinsky and Saxena* [1997] data. The α profile obtained with $\alpha(P = 0) = 4.75\times10^{-5}$ K^{-1}, and δ_T=5.5 [*Chopelas*, 1990], together with theoretical profiles at 940 K [*Inbar and Cohen*, 1995] and at 1000 K [*Isaak et al.*, 1990] is also plotted.

which is equivalent to

$$\alpha(P,T) \simeq (3.0 \times 10^{-5} + 1.2 \times 10^{-8}T) \times (1 - 0.024P + 2.2 \times 10^{-4}P^2),$$

with P in GPa and T in K, which gives $\alpha_0 = 3.02 \times 10^{-5}$ K^{-1} and $\alpha_1 = 1.2 \times 10^{-8}$ K^{-2}.

The value of $(\partial K_T/\partial T)_P$ computed by the use of the identity $(\partial K_T/\partial T)_P = K_T^2(\partial\alpha/\partial P)_T$ is -0.024(5) GPa K^{-1}, which is in good agreement with the former analysis, showing that $(\partial K_{0,T}/\partial T)_P$ does not depend strongly on the choice of the high P and high T EoS. At 1000 K and ambient pressure the corresponding value of $\delta_T = -1/\alpha K_T(\partial K_T/\partial T)_P$ is 4.4 ± 1.

Chopelas [1990] obtained that δ_T is constant ($\delta_T \simeq 5.5$) above the Debye temperature and at pressures up to 30 GPa. This leads to the thermal expansion coefficient profile plotted in Figure 3 (calculated with $\alpha(P = 1 \text{ bar}, T) = 4.75 \times 10^{-5}$ K^{-1}), which is in correct agreement with our measurements. Besides, *Inbar and Cohen* [1995] computed a thermal expansivity which is slightly higher that what we measured ($\simeq 20\%$ at 50 GPa) at 940 K, when the *Isaak et al.* [1990] quasi-harmonic estimate at 1000 K is roughly equal to Chopelas's law for $P > 10$ GPa.

4.2. Debye-Mie-Grüneisen Formalism

The Debye-Mie-Grüneisen EoS can also be used to compute $P(V,T)$. The Mie-Grüneisen formalism relies on the assumption that the free energy and the pressure can be divided into two terms:

$$P(V,T) = P_{\text{stat}}(V, T = 0) + P_{th}(V,T), \quad (3)$$

where P_{th}, the thermal pressure, is created by thermal motion of atoms in the lattice. Classically, P_{th} is related to the thermal energy E_{th} by [see *Poirier*, 1991]:

$$P_{th}(V,T) = \frac{\gamma}{V}E_{th}(V,T), \quad (4)$$

where γ is the thermodynamic Grüneisen parameter ($\gamma = \alpha K_S V/C_P$). E_{th} can be calculated using the quasi-harmonic Debye theory:

$$E_{th}(T,\theta_D) = 9nRT\left(\frac{T}{\theta_D}\right)^3 \int_0^{\theta_D/T} \frac{x^3}{e^x - 1}dx, \quad (5)$$

where $n = 2$ for MgO. Within the quasi-harmonic approximation, the Debye temperature θ_D is a function of volume only. It can be shown that $d\ln\theta_D/d\ln V = -\gamma$, and the following volume dependence of γ is generally assumed: $\gamma = \gamma_0(V/V_0)^q$ [see *Poirier*, 1991]. Using the database of *Anderson and Zou* [1989], the value of θ_{D0} can be estimated by fitting theoretical Debye $C_V = (\partial E_{th}/\partial T)_V$ with experimental measurements. A value of $\theta_{D0} = 800 \pm 50$ K is obtained, compatible with previous estimates using the same model [*Jamieson et al.*, 1982].

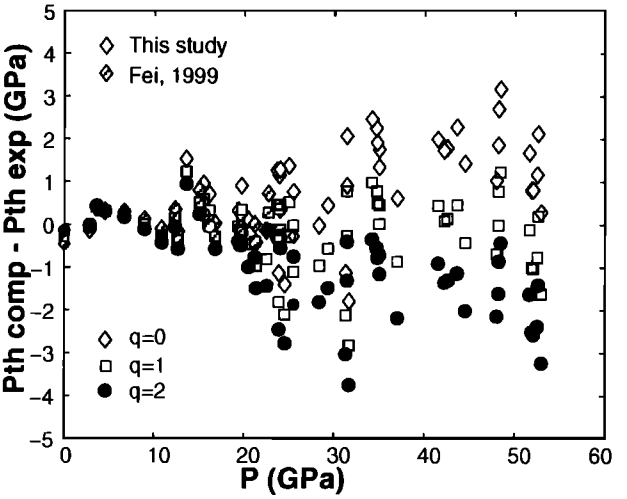

Figure 4. Computed difference between $P_{\text{th comp}} = P(V,T) - P(V, 300 \text{ K})$ estimated from the Debye model, with $\gamma_0 = 1.45$, $\theta_{D0} = 800$ K (for 3 values of q), and $P_{\text{th exp}} = P(V,T) - P_{BM}(V, 300)$ for the present measurements and *Fei* [1999] measurements. *Utsumi et al.* [1998] data ($P < 10$ GPa) are not represented because they do not constrain the q value.

The preceding relations allow one to express the pressure as a function of V, T, $\theta_{D0} = \theta_D(V = V_0)$, $\gamma_0 = \gamma(V = V_0)$ and q, namely,

$$P(V,T) - P(V,T_0) = \frac{\gamma(V)}{V}(E_{th}(V,T) - E_{th}(V,T_0)). \quad (6)$$

The values of γ_0 and q have to be determined; they can be constrained by plotting $P(V,T) - P_{BM}(V, T_0 = 300$ K), the difference between the thermal pressure computed with the Debye model and the thermal pressure deduced from our data set (see Figure 4). The zero pressure value of P_{th} depends strongly on γ_0 (it allowed us to fix $\gamma_0 = 1.45 \pm 0.1$), whereas q essentially influences its variations with pressure. It is obvious from the scatter of the data that q can not be better constrained than $q = 0.8 \pm 0.5$.

The above show that a simple Debye model, with a temperature-independent γ value and a constant q value is sufficient to describe the experimental measurements in the pressure and temperature range investigated. This result confirms the analysis carried out by *Anderson* [1995, pp. 111-156] which showed that MgO is a Debye-like solid on the basis of the values of θ_D and γ determined by both acoustic and calorimetric measurements. Moreover, the acoustic γ_0 value (1.5) reported by *Anderson* [1995] is in good agreement with our estimate, which is based on an independent method.

4.3. Comparison and Discussion

A most sensitive way to compare the high T Birch-Murnaghan and Mie-Grüneisen EoS is to plot thermal pressure $P(V,T) - P(V,T_0)$ as a function of volume, because the ambient temperature compressional behavior

Table 5. Set of parameters for the high-T and high-P EoS that are used for the thermal pressure calculations plotted on figure 5 .

Parameter	Value		
	T-dependent B.M. EoS; set 1	T-dependent B.M. EoS; set 2	Mie-Grüneisen EoS
V_0, Å^3	74.71	74.71	74.71
K_0, GPa	161	161	161
K'_0	3.94	3.94	3.94
$\partial K_T/\partial T$, GPa K^{-1}	-0.022	-0.026	
α, K^{-1}	2.9 +0.0012 T	2.9 +0.0012 T	
θ_{D0}, K			800
γ_0			1.45
q			0.8

is eliminated by evaluating the thermal pressure. P_{th} estimated from the Debye model, with parameters listed in Table 5, for T up to 3000 K, is plotted on Figure 5. The volume effect on P_{th} is slight, in that case (q=0.8) and when q varies between 0.5 and 1.5. P_{th} is roughly proportional to the temperature difference, $T - T_0$. We assume here that P_{th} estimated from the Debye model is correct.

$P_{th} = P_{BM}(V,T) - P_{BM}(V,T_0)$ is also plotted for the same conditions, using two parameter sets (Table 5): set 1 resulting from inversion of our data alone and set 2 including all data. P_{th} curves evaluated from set 2 show an anomalous behavior at low V (high P), as negative P_{th} are forbidden for materials having a positive thermal expansion coefficient. A value of $(\partial K_{0,T}/\partial T)$ of -0.026 GPa K^{-1} or higher thus appears inadequate, if $K'_{0,T}$ is assumed to be constant. In contrast, P_{th} estimated from set 1 agrees (less than 2 GPa difference) with Debye model calculation.

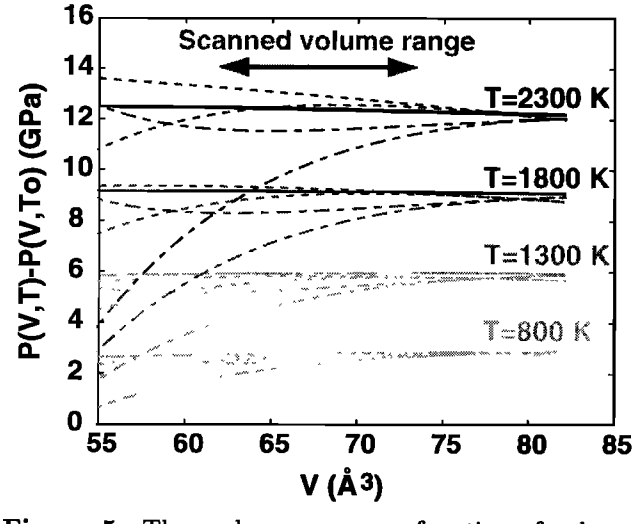

Figure 5. Thermal pressure as a function of volume, for various temperatures (800 to 2300 K) plotted in different shades. For each temperature, five thermal pressures are plotted. Solid line represents $P(V,T) - P(V,T_0)$ estimated from the Debye model. Dashed and dot-dashed lines represent $P_{BM}(V,T) - P_{BM}(V,T_0)$, with the parameters of sets 1 and 2 from the Table 5, respectively. For these estimates, lower curves correspond to $(\partial K'_T/\partial T)_P = 0$, and upper dot-dashed and dashed curves correspond to $(\partial K'_T/\partial T) = 2\times10^{-4}$ K^{-1} and $(\partial K'_T/\partial T) = 6 \times 10^{-5}$ K^{-1}, respectively.

The curvature in the P_{th} profiles which appears at high compression shows that $K'_{0,T}$ increases with temperature. A value of $(\partial K'_T/\partial T) = 6 \times 10^{-5}$ K^{-1} is sufficient to reconcile the profile estimated from set 1 with the Debye profile (Figure 5). The $K'_{0,T}$ temperature derivative estimated by *Isaak et al.* [1990]; (3×10^{-4}) is much higher. On the other hand, if we assume that $(\partial K'_T/\partial T) = 2 \times 10^{-4}$ K^{-1}, $(\partial K_{0,T}/\partial T)$ = -0.026 GPa K^{-1} becomes possible. Thus temperature effect on $K'_{0,T}$ remains poorly constrained, even if the present study indicates that $K'_{0,T}$ increases with temperature, which confirms *Isaak et al.*'s [1990] conclusions.

The main conclusions of this study are (1) a quasi-harmonic Debye theory can correctly describe our P-V-T measurements, up to 53 GPa and 2474 K; this shows that the thermal behavior of periclase under high pressure can be easily calculated; (2) the parameters of this EoS are K_0 = 161 GPa, K'_0 = 3.94±0.3, V_0 = 74.71 Å^3, θ_{D0} = 800 K, γ_0 = 1.45 and $q = 0.8 \pm 0.5$, compatible with $(\partial K_T/\partial T)_P = -0.022$ GPa K^{-1}; (3) the difficulties in pressure extrapolation, at low or high temperature, show that volume measurements at higher pressure seem necessary to obtain high-accuracy (less than 0.1% error) equation of state in the whole lower mantle pressure range; (4) $K'_{0,T}$ increases with T, but the current data do not allow to quantitatively estimate this dependence.

Acknowledgments. We thank J. Matas for providing the global inversion code. Comments by Russel Hemley, Yingwei Fei, and Donald Isaak greatly improved this report. We thank G. Montagnac, T. LeBihan, and M. Mezouar for their help during the experiments.

References

Anderson, O. *Equations of State of Solids for Geophysics and Ceramic Science*, Oxford Univ. Press, New York, 1995.

Anderson, O., and K. Zou, Formulation of the thermodynamic functions for mantle minerals: MgO as an example, *Phys. Chem. Miner.*, *16*, 642–648, 1989.

Anderson, O., D. Isaak, and H. Oda, High-temperature elastic constant data on minerals relevant to geophysics, *Rev. Geophys.*, *30*, 57–90, 1992.

Andrault, D., G. Fiquet, J.-P. Itié, P. Richet, P. Gillet, D. Hausermann, and M. Hanfland, Thermal pressure in the laser-heated diamond-anvil cell: An X-ray diffraction study, *Eur. J. Mineral.*, *10*, 931–940, 1998.

Barrett, C., and L. Meyer, Argon-nitrogen phase diagram, *J. Chem. Phys.*, *42*, 107–112, 1965.

Chen, G., R. Liebermann, and D. Weidner, Elasticity of single-crystal MgO to 8 Gigapascal and 1600 K, *Science*, *280*, 1913–1916, 1998.

Chervin, J.C., B. Canny, J.M. Besson, and J.M. Pruzan, A diamond anvil cell for IR microspectroscopy, *Rev. Sci. Instrum.*, *66*, 2595–2598, 1995.

Chopelas, A., Thermal expansion, heat capacity, and entropy of MgO at mantle pressures, *Phys. Chem. Miner.*, *17*, 142–148, 1990.

Dewaele, A., G. Fiquet, and P. Gillet, Temperature and pressure distribution in the laser-heated diamond-anvil cell, *Rev. Sci. Instrum.*, *69*, 2421–2426, 1998.

Dubrovinsky, L., and S. Saxena, Thermal expansion of periclase (MgO) and tungsten (W) to melting temperatures, *Phys. Chem. Miner.*, *24*, 547–550, 1997.

Duffy, T., and T. Ahrens, Compressional sound velocity, equation of state, and constitutive response of shock-compressed magnesium oxide, *J. Geophys. Res.*, *100*, 529–542, 1995.

Duffy, T., R. Hemley, and H.-K. Mao, Equation of state and shear strength at multimegabar pressures: Magnesium oxide to 227 GPa, *Phys. Rev. Lett.*, *74*, 1371–1374, 1995.

Fei, Y., Effect of temperature and composition on the bulk modulus of (Mg,Fe)O, *Am. Mineral.*, *84*, 272–276, 1999.

Fei, Y., H.-K. Mao, J. Shu, and J. Hu, P-V-T equation of state of magnesiowüstite $(Mg_{0.6}Fe_{0.4})O$, *Phys. Chem. Miner.*, *18*, 416–422, 1992.

Fiquet, G., D. Andrault, J.-P. Itié, P. Gillet, and P. Richet, X-ray diffraction of periclase in a laser-heated diamond-anvil cell, *Phys. Earth Planet. Inter.*, *95*, 1–17, 1996.

Fiquet, G., D. Andrault, A. Dewaele, T. Charpin, M. Kunz, and D. Hausermann, P-V-T equation of state of $MgSiO_3$ perovskite, *Phys. Earth Planet. Inter.*, *105*, 21–31, 1998.

Fiquet, G., P. Richet, and G. Montagnac, High temperature thermal expansion of lime, periclase, corundum and spinel, *Phys. Chem. Miner.*, *16*, in press, 1999.

Hammersley, A., Fit2D, *Pub. ESRF98HA01T*, European Synchrotron Radiation Facility, Grenoble, France, 1996.

Inbar, I., and R. Cohen, High pressure effects on thermal properties of MgO, *Geophys. Res. Lett.*, *22*, 1533–1536, 1995.

Isaak, D., O. Anderson, and T. Goto, Measured elastic moduli of single-crystal MgO up to 1800 K, *Phys. Chem. Minerals*, *16*, 704–713, 1989.

Isaak, D., R.E. Cohen, and M.J. Mehl, Calculated elastic and thermal properties of MgO at high pressures and temperatures, *J. Geophys. Res.*, *95*, 7055–7067, 1990.

Ita, J., and L. Stixrude, Petrology, elasticity and composition of the mantle transition zone, *J. Geophys. Res.*, *97*, 6849–6866, 1992.

Jackson, I., and H. Niesler, The elasticity of periclase to 3 GPa and some geophysical implications, in *High Pressure Research in Geophysics*, edited by S. Akimoto and M. Manghnani, pp. 93–114, Cent. for Acad. Publish. of Jp., Tokyo, 1982.

Jamieson, J., J. Fritz, and M. Manghnani, Pressure measurement at high temperature in X-ray diffraction studies: Gold as a primary standard, in *High Pressure Research in Geophysics*, edited by S. Akimoto and M. Manghnani, pp. 27–48, Cent. for Acad. Publish. of Jp., Tokyo, 1982.

Jeanloz, R., and R.J. Hemley, Thermoelasticity of perovskite: An emerging consensus, *Eos Trans. AGU*, *75*, 41, 476–477, 1994.

Karki, B., L. Stixrude, S. Clark, M. Warren, G. Aukland, and J. Crain, Structure and elasticity of MgO at high pressure, *Am. Mineral.*, *82*, 51–60, 1997.

Knittle, E., Static compression measurements of equations of state, in *Mineral Physics and Crystallography: A Handbook of Physical Constants*, AGU ref. Shelf, vol. 2, edited by T.J. Ahrens, pp. 98-142, AGU, Washington, D.C., 1995.

Larson, A., and R.B. Von Dreele, *GSAS Manual*, Los Alamos Nat. Lab. Rep. LAUR 86-748, Los Alamos, 1994.

LeBail, A., *Accuracy in Powder Diffraction*, p. 213, Nat. Inst. of Stand. and Technol., Gaithersburg, Md., 1992.

Mao, H.-K., and P. Bell, Equations of state of MgO and ϵ-Fe under static pressure conditions, *J. Geophys. Res.*, *84*, 4533–4536, 1979.

Mao, H.-K., R. Hemley, Y. Fei, J. Shu, L. Chen, A. Jephcoat, and Y. Wu, Effect of pressure, temperature and composition on lattice parameters and density of $(Mg,Fe)SiO_3$-perovskites to 30 GPa, *J. Geophys. Res.*, *96*, 8069–8079, 1991.

Matas, J., Modélisation thermochimique des propriétés des solides à haute pression et haute température: Applications géophysiques, Ph.D. thesis, École Normale Supér. de Lyon, Lyon, France, 1999.

Mehl, M.J., R.E. Cohen, and H. Krakauer, Linearized augmented plane waves electronic structure calculations for MgO and CaO, *J. Geophys. Res.*, *93*, 8009-8022, 1988.

Mills, R., B. Olinger, and D. Cromer, Structures and phase diagrams of N_2 and CO to 13 GPa by X-ray diffraction, *J. Chem. Phys.*, *84*, 2837–2845, 1986.

Poirier, J., *Introduction to the Physics of the Earth's Interior*, Cambridge Univ. Press, New York, 1991.

Poirier, J.-P., and A. Tarantola, A logarithmic equation of state, *Phys. Earth Planet. Inter.*, *109*, 1–8, 1998.

Richet, P., H.-K. Mao, and P. Bell, Static compression and equation of state of CaO to 1.35 Mbar, *J. Geophys. Res.*, *93*, 15,279–15,288, 1988.

Ross, M., H.-K. Mao, P. Bell, and J. Xu, The equation of state of dense argon: A comparison of shock and static studies, *J. Chem. Phys.*, *85*, 1028–1033, 1986.

Singh, A.K., The lattice strains in a specimen (cubic system) compressed nonhydrostatically in an opposed anvil device, *J. Appl. Phys.*, *73*, 4278-4286, 1993.

Thoms, R., S. Bauchau, M. Kunz, T. LeBihan, M. Mezouar, D. Hausermann, and D. Strawbridge, An improved detector for use at synchrotrons, *Nucl. Instr. and Meth. A*, *413*, 175–180, 1998.

Utsumi, W., D.J. Weidner, and R.C. Liebermann, Volume measurement of MgO at high pressures and high temperatures, in *Properties of Earth and Planetary Materials at High Pressure and Temperature*, Geophys. Monogr. Ser., vol. 101, edited by M.H. Manghnani and T. Yagi, pp. 327–333, AGU, Washington, D.C., 1998.

Vinet, P., J. Ferrante, J. Rose, and J. Smith, Compressibility of solids, *J. Geophys. Res.*, *92*, 9319–9325, 1987.

Wittlinger, J., R. Fisher, S. Werner, J. Schneider, and H. Schulz, High pressure study of hcp-argon, *Acta Crystallogr. B*, *53*, 745–749, 1997.

D. Andrault, Département des Géomatériaux, URA 734, CNRS, Institut de Physique du Globe, 4, place Jussieu, 75252 Paris Cedex 05, France.

A. Dewaele and G. Fiquet, Laboratoire des Sciences de la Terre, UMR 5570, CNRS, École Normale Supérieure de Lyon, 46, allée d'Italie, 69364 Lyon Cedex 07, France. (adewaele@ens-lyon.fr)

D. Hausermann, European Synchrotron Radiation Facility, BP 220, 38042 Grenoble Cedex, France.

(Received February 17, 1999; revised August 17, 1999; accepted October 11, 1999.)